Unveiling the Degradation Nature of $Pt/NbO_x/C$ Catalysts for Oxygen Reduction Reaction via *in situ* X-ray Absorption Spectroscopy

Ershuai Liu[1], Qingying Jia[1], Jun Yang[2], Kai Sun[3], Li Jiao[4], Thomas Stracensky[1], Sanjeev Mukerjee*[,1]

[1] Department of Chemistry and Chemical Biology, Northeastern University, Boston, Massachusetts, 02115, United States

[2] Ford Motor Company, Dearborn, MI, 48121, United States

[3] Department of Materials Science and Engineering, University of Michigan, Ann Arbor, MI, 48109, United States

[4] Department of Chemical Engineering, Northeastern University, Boston, Massachusetts, 02115, United States

*Correspondence author email: s.mukerjee@northeastern.edu

Abstract

Among various metal nanoparticles supported on metal oxide (MMO) catalysts, the Pt/NbO_x/C system has promising oxygen reduction reaction (ORR) activity as cathode for proton exchange membrane fuel cells (PEMFCs). Herein, we study a series of Pt/NbO_x/C catalysts with tunable structural and electronic properties via physical vapor deposition and unravel the nature of metal and metal oxide interaction (MMOI) by characterizing this system under reactive conditions. By conducting *in situ* X-ray absorption spectroscopy (XAS) experiments, we demonstrate the Pt preferably interacts with O but not Nb in the Pt/NbO_x/C system and such Pt-O interaction benefits the ORR activity via electronic effect rather than strain effect. We also provide clear evidence for the formation of metallic Nb phase at the early stage of PEMFC operation and identify severe particle growth of Pt after long-term PEMFC operation. These findings deepen our understanding of the degradation mechanism of MMO catalysts during long-term PEMFC operation.

Keywords ORR, Pt, MMO catalyst, PEMFC, XAS

Widespread application of proton exchange membrane fuel cells (PEMFCs) requires low cost, high activity, and robust electrocatalysts for oxygen reduction reaction (ORR). The ORR in acid electrolyte (Eq.1) is a slow four-electron transfer process resulting in high overpotentials at the cathodes of PEMFCs.

$$O_2 + 4H^+ + 4e^- \rightarrow 2H_2O \quad \text{(Eq.1)}$$

The development of PEMFCs therefore requires the synthesis of advanced ORR catalysts, which makes electricity efficiently by the electrochemical oxidation of hydrogen fuel at their anodes and reduction of oxygen at their cathodes. The specific activity of Pt electrocatalysts can be enhanced through what is known as the strong metal support interaction (SMSI)[1,2], either with a carbon support[3] or with transition metal oxide support[4] . However, most of the carbon supported Pt-based catalysts suffers from carbon corrosion[5–7] and Pt dissolution[8] under operating conditions, which leads to the loss of electrochemical active area and PEMFC performance degradation[9]. To alleviate these issues, many efforts have been devoted to tuning the interactions between Pt and the support, nanoparticles crystal orientation engineering, and crystallinity of carbon nanoparticles[10]. Incorporating conductive metal oxide to form metal particles supported on metal oxides (MMO) can alternatively eliminate carbon corrosion. It has been well documented that the Pt deposited on metal oxides such as NbO_x (x=1, 2, 2.5) exhibits 2 to 3 times higher ORR activity compared to bare Pt[4,11] and meanwhile NbO_x helps to stabilize the Pt with enhanced durability[12]. Despite the significant enhancement on the ORR activity of Pt, the catalytic roles of NbO_x support have still been elusive.

Herein, we aim to unravel the nature of the interfacial metal and metal oxide interaction (MMOI) of $Pt/NbO_x/C$ and correlate such interaction to the beneficial effect of NbO_x support on ORR. To pursue this, we probe MMOI on $Pt/NbO_x/C$ systems prepared via magnetron sputtering

method by Exothermics *Inc* (details can be found in our previous work[13]). We employ *in situ* X-ray absorption spectroscopy (XAS) together with complementary techniques including electrochemical characterization and microscopy to investigate the nature of MMOI in $Pt/NbO_x/C$ systems with tunable interface morphologies.

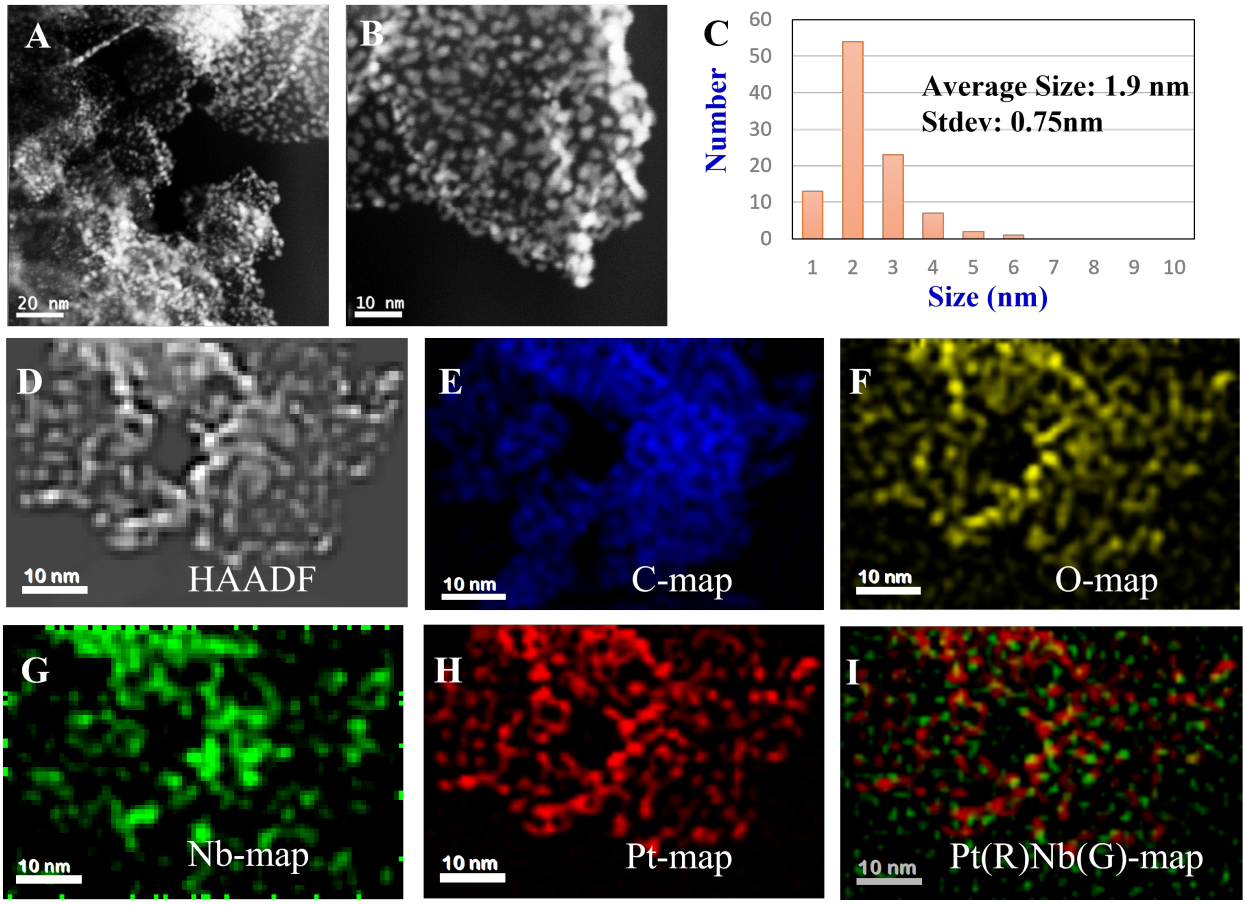

Figure 1 (A-B) HAADF-STEM images at different magnifications, (C) particles diameter distribution, (D) HAADF-STEM image, EDS mapping of (E) carbon, (F) oxygen, (G) niobium, (H) platinum and (I) platinum mixed with niobium (red represents Pt, green represents Nb) of catalyst PtNb-0.17.

We first utilized High-Angle Annular Dark Field Scanning Transmission Electron Microscopy (HAADF-STEM) and its Energy Dispersive X-ray Spectroscopy (EDS) to visualize the morphology of a series of $Pt/NbO_x/C$ catalysts. All the $Pt/NbO_x/C$ samples are named via PtNb-X, X represents the Nb/Pt atomic ratio measured by X-ray Photoelectron Spectroscopy

(XPS, **Table S2**). For the sample PtNb-0.17, the Pt nanoparticles were dispersed on NbO_x substrate homogeneously (**Figure 1 A-B**). The particle size ranges from 1-6 nm with an average size of 1.9 nm (**Figure 1C**). EDS mapping further confirms that the relatively uniform structures were accomplished by this magnetron sputtering method (**Figure 1D-I**). XPS experiments were later conducted to identify the oxidation states of the Pt and Nb located in the near-surface region. In addition, the counterpart Pt/C without the presence of NbO_x (denoted as Pt baseline) and the NbO_x/C without the presence of Pt (denoted as NbO_x) was also studied as baselines. **Figure 2A** and **Figure 2B** show the Nb 3d XPS spectra of the NbO_x and PtNb-0.17, respectively. The Nb peaks of the NbO_x sample without the presence of Pt has a higher energy than that of all samples with Pt (**Figure 2C**), which indicates that the presence of Pt enriches the electrons of NbO_x . **Figure 3D** and **Figure 3E** show the Pt 4f XPS spectra of Pt baseline and PtNb-0.17. The Pt peaks of Pt baseline without the presence of NbO_x has a lower energy than that of other samples with the presence of NbO_x (**Figure 2F**), which indicates that the presence of NbO_x makes the coexist Pt electron deficient. These results together verify the electron transfer from Pt to NbO_x. The extent of the electron transfer must be mild since the oxidation state of neither the Pt^0 nor the Nb^{5+} changes significantly in all studied Pt/NbO_x/C catalysts.

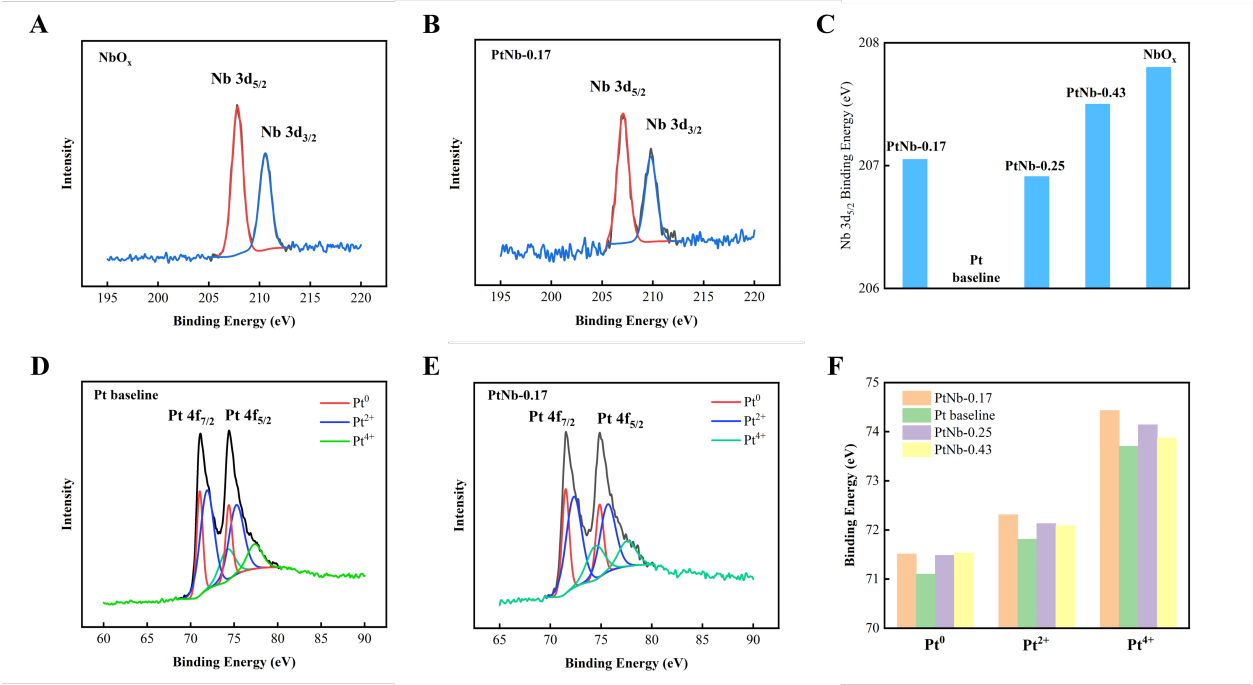

Figure 2 Nb 3d XPS spectra of (A) NbO_x and (B) sample PtNb-0.17. (C) Summary of the Nb 3d binding energy of all studied samples. Pt 4f XPS spectra of (D) sample Pt baseline and (E) sample PtNb-0.17. (F) Summary of the Pt 4f binding energy of all samples (the peak positions of Pt^0, Pt^{2+} and Pt^{4+} are based on the fitting results).

The Nb K-edge X-ray absorption near-edge structure (XANES) spectra and the Fourier-Transform of the extended X-ray absorption fine structures (FT-EXAFS) of these samples (except for Pt baseline that does not contain Nb) are presented in **Figure 3A** and **Figure 3B**, respectively. The Nb K-edge XANES spectra of all tested $Pt/NbO_x/C$ samples nearly overlap that of the Nb_2O_5 standard and are away from that of the and PtNb alloy and NbO_2 standards (**Figure 3A**). These results show that the bulk average oxidation state of the Nb in these $Pt/NbO_x/C$ samples are all close to +5. Note that unlike XAS that is a bulk average technique, XPS is surface sensitive and probes the elements in the near-surface region (~1 nm depth). Thus, the slightly unsaturated oxidation state of the Nb detected by XPS in combination with the nearly +5 oxidation state measured by XAS suggest that the surface Nb has an oxidation state lower than +5 whereas the inner Nb has an oxidation state of +5. The FT-EXAFS peaks of the $Pt/NbO_x/C$ samples nearly

overlap that of the Nb_2O_5 (**Figure 3B**), in line with the XANES spectra. The presence of two peaks of PtNb-0.25 suggests the presence of a small amount of NbO_2. The absence of the Nb-Pt scattering peak around 2.2 Å that was previously observed in the PtNb alloy[14] and signifies the lack of Nb-Pt alloying phase or the Nb-Pt interactions are too weak to be detected by FT-EXAFS. Unlike the XPS measurements, there is no clear trend in the XANES or FT-EXAFS spectra of tested $Pt/NbO_x/C$ samples as a function of the Nb content. Considering the bulk average nature of XAS, we attribute this to the majority of the Nb might be in the inner part of catalyst particles without exposed to air or in contact with Pt.

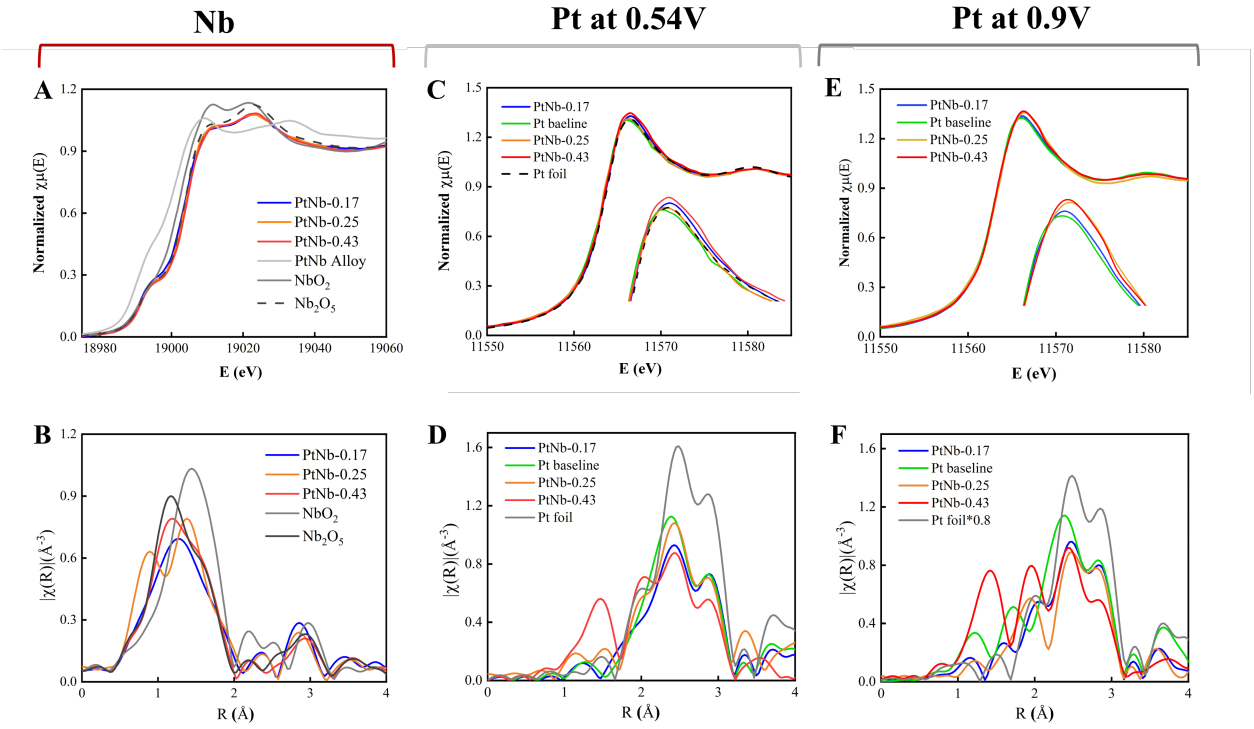

Figure 3 The *ex situ* Nb K-edge (A) XANES spectra and (B) FT-EXAFS spectra of different $Pt/NbO_x/C$ samples. The *in situ* Pt L_3-edge (C) XANES and (D) FT-EXAFS spectra at 0.54V. The *in situ* Pt L_3-edge (E) XANES and (F)FT-EXAFS spectra at 0.9V. All *in situ* data were collected in an O_2-saturated 0.1 M $HClO_4$ electrolyte.

To further investigate the Pt-Nb interaction under reactive conditions, we conducted *in situ* XAS experiments on listed $Pt/NbO_x/C$ samples at the Pt L_3-edge at 0.54 V and 0.90 V (**Figure 3C-F**). These two potentials are mostly important in terms of ORR: 0.54 V is located at the double

layer region so the Pt surface can be presumably considered clean devoid of hydrogen and oxygen adsorbates; 0.90 V is the potential where the ORR activity of Pt-based catalysts is normally evaluated. For both potentials, the white line intensity of the Pt XANES main peak around 11567 eV at 0.54 V generally increases with increasing Nb content. This major peak arises from the electron transition from 2p to 5d orbitals. Thus, a higher white line intensity means a higher transition probability and a more unoccupied 5d orbital or equivalently less 5d electrons[15]. This trend therefore indicates that increasing Nb content reduces the number of 5d electrons of Pt, signifying the electron transfer from Pt to Nb, in consistent with the trend derived from XPS.

In addition, the intensity of the FT-EXAFS peak around 2-3 Å arisen from the first shell Pt-Pt scattering generally decreases with higher Nb content (**Figure 3D**). The EXAFS fitting also shows that the PtNb-0.17 with the lowest Nb content has the largest Pt-Pt coordination number (**Table S3**). In particular, the PtNb-0.43 has not only the lowest peak intensity, but also another peak around 1.5 Å that is normally assigned to the Pt-O interaction. Since the O observed at 0.54V cannot be generated from water dissociation that occurs above at 0.7 V, we attribute this peak to the interaction between the Pt and the O from NbO_x. Thus, the Pt interacts with the O rather than Nb of the NbO_x underneath. This is further supported by the lack of Pt-Nb interaction observed from the FT-EXAFS from both the Pt (**Figure 3D**) and Nb (**Figure 3B**) perspective. This configuration is consistent with the near saturation of the oxidation state of the NbO_x in which the Nb is fully surrounded by O neighbors. This Pt-O peak further grows up when the applied potential elevates to 0.9V, which can be ascribed to water dissociation. On the other hand, we previously showed that direct Pt-Nb interactions can be clearly observed only when the bulk average oxidation state of the NbO_x is significantly lower than +5 that leads to large amounts of oxygen vacancies[16].

EXAFS fitting results show that the first-shell Pt-Pt bond lengths of the Pt/NbO_x/C samples are comparable to that of the Pt reference foil (**Table S3**). This indicates that the presence of NbO_x does not change the lattice constant of Pt notably, thereby ruling out the compressive-strain effect induced by NbO_x. This is expected from the lack of direct Pt-Nb interactions as Nb atom is bigger than Pt atom. Therefore, the superior ORR activity of Pt/NbO_x/C to that of the counterpart Pt/C cannot be ascribed to the Nb-induced strain effect. On the other hand, we attribute it to the Nb-induced electronic effect. More concretely, it has been demonstrated that Pt binds O 0.1 eV overly strong and its ORR activity can be improved by weakening the Pt-O bonds[17]. The minor electron transfer from Pt to the O in the co-present NbO_x suppresses the electron transfer from the same Pt to the O from the O_2 or ORR intermediates, thereby improving the ORR activity. Surface sensitive Δμ-XANES analysis (details in Supplementary Information, **Figure S4**) also suggests that the presence of NbO_x might change the shape of Pt clusters making a higher fraction of Pt atoms exposed to air.

The catalyst PtNb-0.17 exhibits best ORR performance in rotating disk electrode (RDE) among studied samples (**Figure S5**). We therefore conducted membrane electrode assembly (MEA) evaluation coupling with *in situ* XAS to understand the origins of its ORR activity and degradation. The XAS electrodes are made by the PtNb-0.17 powders, as well as on the cathode of cycled MEAs. Specifically, after the MEA was evaluated in a PEMFC, the cathode was peeled off from the MEA and transferred into a XAS flow cell for *in situ* XAS measurements, similar to our previous work [18]. This method effectively correlates the XAS derived structural and electronic properties to the activity and durability evaluated in MEAs.

Like all the Pt/NbO_x/C catalysts reported above, the Nb in the PtNb-0.17 powders without assembled into a MEA (denoted as fresh) is mainly in the form of Nb_2O_5, which is clearly

evidenced by the observation that its XANES (**Figure 4A**) and FT-EXAFS (**Figure 4B**) spectra nearly overlap those of the Nb_2O_5 standard. However, upon the MEA operation in a PEMFC for ~200 cycles (beginning of life, denoted as MEA-BOL), the XANES spectrum slightly shifts to lower energy toward that of the Nb reference foil. Meanwhile, a small FT-EXAFS scattering peak around 2.5 Å overlapping that of the Nb reference foil appears (**Figure 4B**). These results together indicate formation of metallic Nb^0 upon short-term MEA operation. Although this is not astonishing considering that Nb_2O_5 is a reducible oxide[19], it is unexpected that Nb^0 forms at such an early stage. After long-term PEMFC operation (end of life, denoted as MEA-EOL), the XANES spectrum further shift negatively to lower energy (**Figure 4A**), and the first derivative XANES spectrum evolves from that of Nb_2O_5 to that of Nb^0 correspondingly, as highlighted by red arrows (**Figure 4C**). Meanwhile, the Nb-Nb scattering peak grows, and perfectly overlaps that of the Nb reference foil in the real R-space (**Figure S6**). These results provide definitive evidence for the formation of Nb^0 upon MEA operation. This phenomenon is believed to be detrimental to MEA performance not only because it will destroy the Pt-NbO_x bonding, but also cause proton starvation (Eq.2) on the membrane due to the possible Nb^0 migration.

$$NbO_x + 2x\ H^+ + 2x\ e^- \rightarrow Nb^0 + xH_2O \qquad \text{(Eq.2)}$$

Although the amount of newly formed Nb^0 shall be small according to the low intensity Nb-Nb scattering peak and the detrimental effect may be minor for Pt/NbO_x/C systems, we consider such phenomenon may be a common concern for most metal support interactions (SMSI) systems composed of reducible oxides.

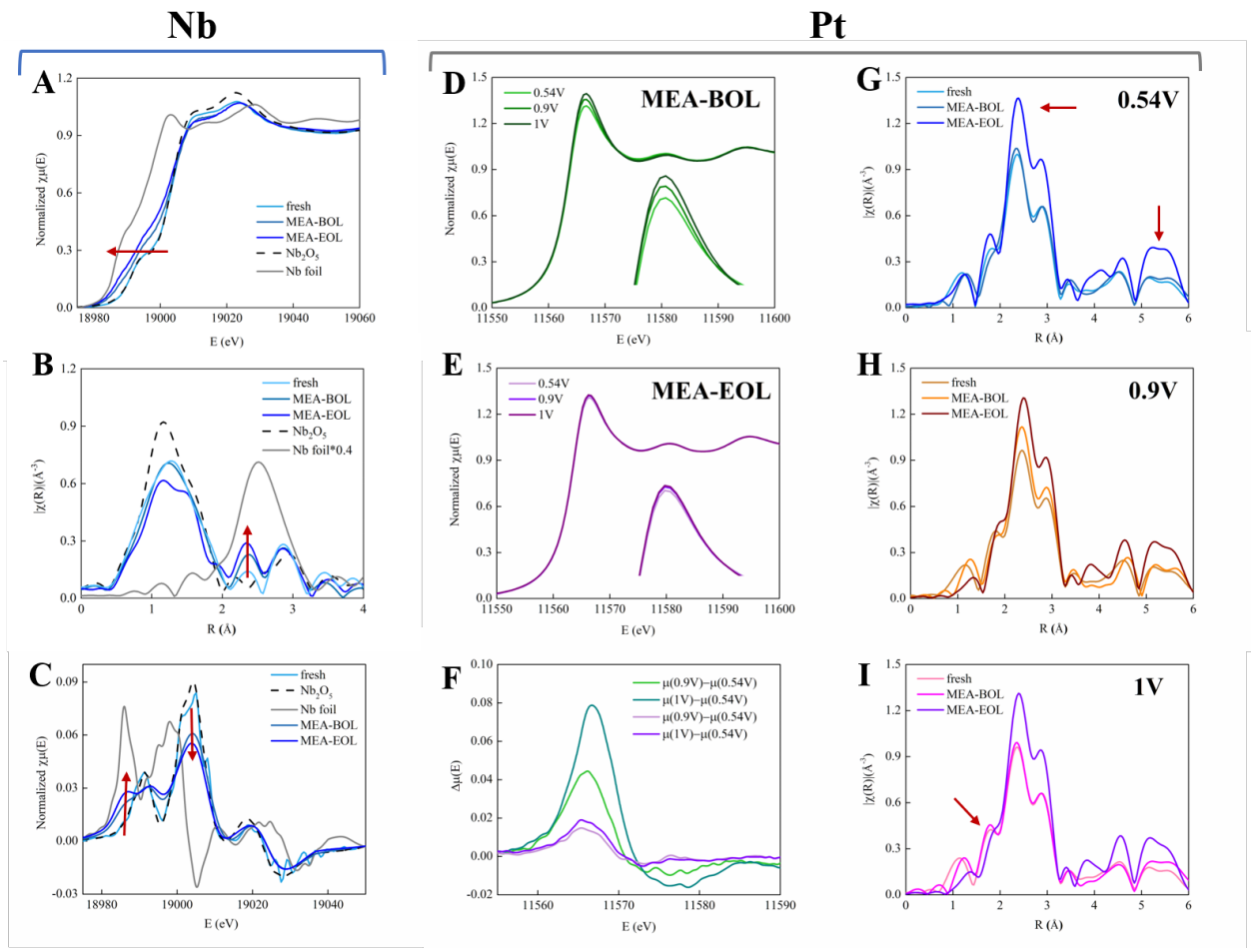

Figure 4. (A) *Ex situ* XANES spectra and (B) *ex situ* FT-EXAFS spectra of the different samples made by PtNb-0.17 at Nb K-edge, together with the Nb_2O_5 and Nb reference foil for comparison. (C) *Ex situ* first derivative XANES spectra of different samples made by PtNb-0.17, together with Nb_2O_5 and Nb reference foil for comparison. *In situ* XANES spectra at the Pt L_3-edge of (D) MEA-BOL and (E) MEA-EOL cathodes peeled from MEAs made by PtNb-0.17, with zoomed region of white line intensity. (F) The derived Δμ-XANES spectra of MEA-BOL (olive and light green) and MEA-EOL (violet and light purple). *In situ* FT-EXAFS spectra of different samples made by PtNb-0.17 at Pt L_3-edge under (G) 0.54V, (H) 0.9V and (I) 1V. All *in situ* data were collected in an O_2-saturated 0.1 M $HClO_4$ electrolyte.

According to the *in situ* XANES spectra of all aforementioned samples, the Pt white line intensity of both the fresh and MEA-BOL samples increases with elevating potentials (**Figure 4D** and **S6**), indicating the progressive growth of the oxygen coverage on the Pt surface with increasing potentials[20,21]. On the other hand, the white line intensity of the MEA-EOL remains nearly unchanged with increasing potentials (**Figure 4E**). The derived Δμ signals of fresh and MEA-BOL

samples are comparable to previously reported Pt-based catalysts[22], whereas the derived Δμ signals of MEA-EOL are minimal in comparison with those of the MEA-BOL (**Figure 4F**). Such observation of MEA-EOL is due to the particle growth that makes surface (electrochemical active) Pt less than that of the MEA-BOL. The *in situ* FT-EXAFS spectra at the Pt L_3-edge of all samples collected at 0.54V, 0.9V and 1.0V are displayed in **Figure 4G-I**. The intensities of the first-shell Pt-Pt scattering peaks between 2.0-3.3 Å of the fresh sample and of the MEA-BOL are comparable, and do not change dramatically with increasing potential (**Figure 4G-I**). These results indicate that the overall structure of the PtNb-0.17 catalyst does not change dramatically in the MEA-BOL and is not subject to heavy O coverage in the MEA even at 1.0 V. This conclusion is supported by the observation that the Pt-O scattering peak around 1.7 Å grows only slightly with increasing potentials (**Figure 4I**), indicating minor oxygen coverage growth. On the other hand, the Pt-Pt scattering peak intensity of the MEA-EOL sample is clearly higher than that of MEA-BOL (**Figure 4G**), indicating the increase in the coordination number. This is quantitatively confirmed by the EXAFS fittings (**Table S4)**. The coordination number increases from 10.6 in the MEA-BOL to 12 in the MEA-EOL. It is noted that the coordination number of 12 is the upper limit for Pt and equal to that of the Pt reference foil (**Table S4**). Since the coordination number of small particles decreases with particle size[23,24], this result demonstrates the growth of the particles of PtNb-0.17 upon long-term PEMFC operation, in consistent with the XANES results. The average particle size in the MEA-EOL shall be bigger than 4 nm since the 4 nm is the lower limit of spherical particles that has a the bulk average coordination number is around 12[25,26], essentially the same as that of the reference foil. Such particle size is at least two times larger than the pristine size (~1.9 nm) observed by HAADF-STEM (**Figure 1C**).

Our observations of the particle growth and Nb reduction of the Pt/NbOx/C catalyst system during long-term PEMFC operation via XAS are consistent with similar studies via HAADF-STEM and Electron Energy Loss Spectroscopy (EELS) from Botton's group[27]. The more dramatical change of Pt nanoparticle size and Nb valence in our work can be ascribed to the more severe environment in PEMFC compared to RDE. It is possible that the reduction of NbO_x promotes the particle growth of Pt since the overall SMSI will be weakened once part of NbO_x converts to Nb^0 that cannot host Pt, which causes agglomeration and sintering of Pt (**Scheme 1**). Strasser's group recently also proposed that the decayed ORR activity of MMO catalysts (Pt/In-Sn oxide and Pt/Ru-Ti oxide) after 0.60-0.95V cycles is due to the formation of oxide overlayer that encapsulates Pt caused by SMSI decoration effect[28,29], which reduces the O_2 accessibility of Pt. However, the missing Pt-Nb interaction and Pt-O interaction (**Figure 4**) suggest that severe particle growth should be the dominant reason for the activity loss in our case. Therefore the reduced availability of surface Pt in $Pt/NbO_x/C$ system results in ORR activity loss during PEMFC operation.

Scheme 1. Structure Changes of Pt and NbO_x Before and After PEMFC Operation

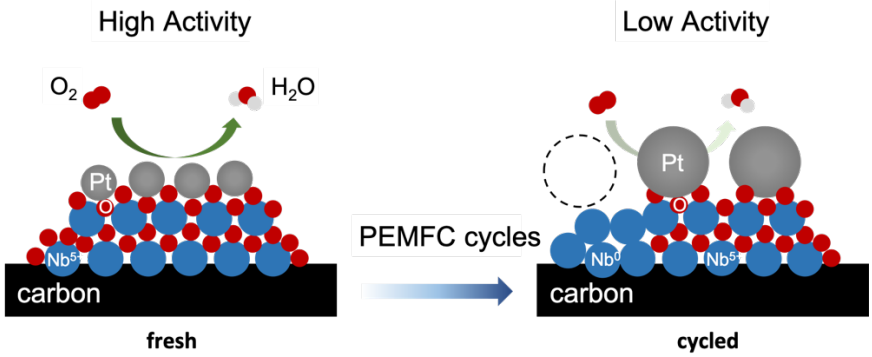

Silver, blue, red and light grey balls represent Pt, Nb, O and H atoms, respectively. The ORR activity decreases as the Pt nanoparticles grow and the newly formed Nb^0 phase is unable to support Pt nanoparticles (black dash line).

In summary, we investigated a series of $Pt/NbO_x/C$ catalysts synthesized via the PVD method and found that there is a weak interaction between the Pt and the NbO_x in the $Pt/NbO_x/C$ systems synthesized. The Pt interacts with the O rather than the Nb, in association with weak electron transfer from the Pt to the O, making the Pt slightly electron deficient. This electronic effect may benefit the ORR activity of Pt by weakening the binding energy between the Pt and the oxygen from the ORR intermediates. Another possible beneficial role of the NbO_x is that it may expose more Pt on surface by changing the Pt cluster morphology, thereby increasing the Pt utilization. However, these beneficial effects on ORR will be gradually impaired as the NbO_x reduces to Nb^0 and Pt particles grows dramatically during PEMFC operation due to the loss of SMSI.

AUTHOR INFORMATION

Corresponding Author

*Sanjeev Mukerjee (s.mukerjee@northeastern.edu)

Notes

The authors declare no competing financial interests.

Author Contributions

E.L., L.J. and T.S. conducted the *in situ* XAS experiments. E.L and Q.J. analyzed the XAS data. J.Y. conducted electrochemical experiments and MEA testing. K.S. conducted TEM and XPS experiments and analyzed data. Q.J. and S.M. supervised and advised the experiments and data analysis. E.L. and Q.J. wrote the manuscript.

ACKNOWLEDGEMENT

This work was supported by Fuel Cell Technology Office under the Office of Energy Efficiency and Renewable Energy of the U.S. Department of Energy((DOE), through Contract No. DE-EE0007675. The XAS data of powder samples were collected at beamline 5-BM-D, Advanced Photon Source (APS) supported by the U.S. DOE, Office of Science, Office of Basic Energy Sciences, under Contract No. W-31-109-Eng-38. The XAS data of MEA samples were collected at beamline 7-BM (QAS), National Synchrotron Light Source-II (NSLS-II) a U.S. DOE Office of Science User Facility operated for the DOE Office of Science by Brookhaven National Laboratory under Contract No. DE-SC0012704. The authors thank Lynne Richard and Dr. Praveen Kolla collected some of the XAS data. The authors acknowledge the help from Dr. Qing Ma from DND-CAT, APS at Argonne National Lab, Dr. Lu Ma and Dr. Steven Ehrlich from NSLS-II at Brookhaven National Lab.

References

(1) Friedel, J.; Sayers, C. M. On the Role of D-d Electron Correlations in the Cohesion and Ferromagnetism of Transition Metals. *J. Phys.* **1977**, *38* (6), 697–705.

(2) Tauster, S. J.; Fung, S. C.; Garten, R. L. Strong Metal-Support Interactions. Group 8 Noble Metals Supported on Ti02. *J. Am. Chem. Soc.* **1978**, *100* (1).

(3) Ma, J.; Habrioux, A.; Morais, C.; Lewera, A.; Vogel, W.; Verde-Gómez, Y.; Ramos-Sanchez, G.; Balbuena, P. B.; Alonso-Vante, N. Spectroelectrochemical Probing of the Strong Interaction between Platinum Nanoparticles and Graphitic Domains of Carbon. *ACS Catal.* **2013**, *3* (9), 1940–1950.

(4) Sasaki, K.; Zhang, L.; Adzic, R. R. Niobium Oxide-Supported Platinum Ultra-Low Amount Electrocatalysts for Oxygen Reduction. *Phys. Chem. Chem. Phys.* **2008**, *10* (1), 159–167.

(5) Roen, L. M.; Paik, C. H.; Jarvi, T. D. Electrocatalytic Corrosion of Carbon Support in PEMFC Cathodes. *Electrochem. Solid-State Lett.* **2003**, *7* (1), A19.

(6) Chen, J.; Siegel, J. B.; Matsuura, T.; Stefanopoulou, A. G. Carbon Corrosion in PEM Fuel Cell Dead-Ended Anode Operations. *J. Electrochem. Soc.* **2011**, *158* (9), B1164.

(7) Chen, J.; Hu, J.; Waldecker, J. R. A Comprehensive Model for Carbon Corrosion during Fuel Cell Start-Up. *J. Electrochem. Soc.* **2015**, *162* (8), F878–F889.

(8) Zhang, H.; Haas, H.; Hu, J.; Kundu, S.; Davis, M.; Chuy, C. The Impact of Potential Cycling on PEMFC Durability. *J. Electrochem. Soc.* **2013**, *160* (8), F840–F847.

(9) Arruda, T. M.; Shyam, B.; Lawton, J. S.; Ramaswamy, N.; Budil, D. E.; Ramaker, D. E.; Mukerjee, S. Fundamental Aspects of Spontaneous Cathodic Deposition of Ru onto Pt/C Electrocatalysts and Membranes under Direct Methanol Fuel Cell Operating Conditions: An in Situ X-Ray Absorption Spectroscopy and Electron Spin Resonance Study. *J. Phys. Chem. C* **2010**, *114* (2), 1028–1040.

(10) Trogadas, P.; Fuller, T. F.; Strasser, P. Carbon as Catalyst and Support for Electrochemical Energy Conversion. *Carbon*. Elsevier Ltd August 1, 2014, pp 5–42.

(11) Timperman, L.; Feng, Y. J.; Vogel, W.; Alonso-Vante, N. Substrate Effect on Oxygen Reduction Electrocatalysis. In *Electrochimica Acta*; Pergamon, 2010; Vol. 55, pp 7558–7563.

(12) Ma, Z.; Li, S.; Wu, L.; Song, L.; Jiang, G.; Liang, Z.; Su, D.; Zhu, Y.; Adzic, R. R.; Wang, J. X.; et al. NbOx Nano-Nail with a Pt Head Embedded in Carbon as a Highly Active and Durable Oxygen Reduction Catalyst. *Nano Energy* **2020**, *69*, 104455.

(13) Xu, C.; Yang, J.; Liu, E.; Jia, Q.; Veith, G. M.; Nair, G.; DiPietro, S.; Sun, K.; Chen, J.; Pietrasz, P.; et al. Physical Vapor Deposition Process for Engineering Pt Based Oxygen Reduction Reaction Catalysts on NbOx Templated Carbon Support. *J. Power Sources* **2020**, *451*, 227709.

(14) Ghoshal, S.; Jia, Q.; Bates, M. K.; Li, J.; Xu, C.; Gath, K.; Yang, J.; Waldecker, J.; Che, H.; Liang, W.; et al. Tuning Nb-Pt Interactions to Facilitate Fuel Cell Electrocatalysis. *ACS Catal.* **2017**, *7* (8), 4936–4946.

(15) Mukerjee, S.; Srinivasan, S.; Soriaga, M. P.; McBreen, J. Role of Structural and Electronic Properties of Pt and Pt Alloys on Electrocatalysis of Oxygen Reduction: An In Situ XANES and EXAFS Investigation. *J. Electrochem. Soc.* **1995**, *142* (5), 1409.

(16) Jia, Q.; Ghoshal, S.; Li, J.; Liang, W.; Meng, G.; Che, H.; Zhang, S.; Ma, Z. F.; Mukerjee, S. Metal and Metal Oxide Interactions and Their Catalytic Consequences for Oxygen Reduction Reaction. *J. Am. Chem. Soc.* **2017**, *139* (23), 7893–7903.

(17) Stamenkovic, V. R.; Fowler, B.; Mun, B. S.; Wang, G.; Ross, P. N.; Lucas, C. A.; Markovic, N. M. Improved Oxygen Reduction Activity on Pt3Ni(111) via Increased Surface Site Availability. *Science (80-.).* **2007**, *315* (5811), 493–497.
(18) Miller, T. E.; Davies, V.; Li, J.; Ghoshal, S.; Stavitski, E.; Attenkofer, K.; Mukerjee, S.; Jia, Q. Actualizing In Situ X-Ray Absorption Spectroscopy Characterization of PEMFC-Cycled Pt-Electrodes. *J. Electrochem. Soc.* **2018**, *165* (9), F597.
(19) Tanabe, K. Application of Niobium Oxides as Catalysts. *Catal. Today* **1990**, *8* (1), 1–11.
(20) Mukerjee, S.; Srinivasan, S. Enhanced Electrocatalysis of Oxygen Reduction on Platinum Alloys in Proton Exchange Membrane Fuel Cells. *J. Electroanal. Chem.* **1993**, *357* (1–2), 201–224.
(21) Mukerjee, S.; Srinivasan, S.; Soriaga, M. P.; Mcbreen, J. Effect of Preparation Conditions of Pt Alloys on Their Electronic, Structural, and Electrocatalytic Activities for Oxygen Reduction-XRD, XAS, and Electrochemical Studies. *J. Phys. Chem* **1995**, *99*, 4577–4589.
(22) Jia, Q.; Liang, W.; Bates, M. K.; Mani, P.; Lee, W.; Mukerjee, S. Activity Descriptor Identification for Oxygen Reduction on Platinum-Based Bimetallic Nanoparticles: *In Situ* Observation of the Linear Composition–Strain–Activity Relationship. *ACS Nano* **2015**, *9* (1), 387–400.
(23) Mukerjee, S.; McBreen, J. Effect of Particle Size on the Electrocatalysis by Carbon-Supported Pt Electrocatalysts: An in Situ XAS Investigation. *J. Electroanal. Chem.* **1998**, *448* (2), 163–171.
(24) De Graaf, J.; Van Dillen, A. J.; De Jong, K. P.; Koningsberger, D. C. Preparation of Highly Dispersed Pt Particles in Zeolite Y with a Narrow Particle Size Distribution: Characterization by Hydrogen Chemisorption, TEM, EXAFS Spectroscopy, and Particle Modeling. *J. Catal.* **2001**, *203* (2), 307–321.
(25) Frenkel, A. I.; Yevick, A.; Cooper, C.; Vasic, R. Modeling the Structure and Composition of Nanoparticles by Extended X-Ray Absorption Fine-Structure Spectroscopy. *http://dx.doi.org/10.1146/annurev-anchem-061010-113906* **2011**, *4*, 23–39.
(26) Witkowska, A.; Cicco, A. Di; Principi, E. Local Ordering of Nanostructured Pt Probed by Multiple-Scattering XAFS. *Phys. Rev. B* **2007**, *76* (10), 104110.
(27) Chinchilla, L.; Rossouw, D.; Trefz, T.; Susac, D.; Kremliakova, N.; Botton, G. A. Nanoscale Analysis of Structural and Chemical Changes in Aged Hybrid Pt/NbOx/C Fuel Cell Catalysts. *J. Power Sources* **2017**, *356*, 140–152.
(28) Schmies, H.; Bergmann, A.; Drnec, J.; Wang, G.; Teschner, D.; Kühl, S.; Sandbeck, D. J. S.; Cherevko, S.; Gocyla, M.; Shviro, M.; et al. Unravelling Degradation Pathways of Oxide-Supported Pt Fuel Cell Nanocatalysts under In Situ Operating Conditions. *Adv. Energy Mater.* **2018**, *8* (4), 1701663.
(29) Hornberger, E.; Bergmann, A.; Schmies, H.; Kühl, S.; Wang, G.; Drnec, J.; Sandbeck, D. J. S.; Ramani, V.; Cherevko, S.; Mayrhofer, K. J. J.; et al. In Situ Stability Studies of Platinum Nanoparticles Supported on Ruthenium−Titanium Mixed Oxide (RTO) for Fuel Cell Cathodes. *ACS Catal.* **2018**, *8* (10), 9675–9683.

For Table of Contents Only